Fatigue Crack Growth Analysis Under Spectrum Loading in Various Environmental Conditions

S. MIKHEEVSKIY, G. GLINKA, and E. LEE

The fatigue process consists, from the engineering point of view, of three stages: crack initiation, fatigue crack growth, and the final failure. It is also known that the fatigue process near notches and cracks is governed by local strains and stresses in the regions of maximum stress and strain concentrations. Therefore, the fatigue crack growth can be considered as a process of successive crack increments, and the fatigue crack initiation and subsequent growth can be modeled as one repetitive process. The assumptions mentioned above were used to derive a fatigue crack growth model based, called later as the UniGrow model, on the analysis of cyclic elastic–plastic stresses–strains near the crack tip. The fatigue crack growth rate was determined by simulating the cyclic stress–strain response in the material volume adjacent to the crack tip and calculating the accumulated fatigue damage in a manner similar to fatigue analysis of stationary notches. The fatigue crack growth driving force was derived on the basis of the stress and strain history at the crack tip and the Smith–Watson–Topper (SWT) fatigue damage parameter, $D = \sigma_{max} \Delta \varepsilon / 2$. It was subsequently found that the fatigue crack growth was controlled by a two-parameter driving force in the form of a weighted product of the stress intensity range and the maximum stress intensity factor, $\Delta K^p K_{max}^{1-p}$. The effect of the internal (residual) stress induced by the reversed cyclic plasticity has been accounted for and therefore the two-parameter driving force made it possible to predict the effect of the mean stress including the influence of the applied compressive stress, tensile overloads, and variable amplitude spectrum loading. It allows estimating the fatigue life under variable amplitude loading without using crack closure concepts. Several experimental fatigue crack growth datasets obtained for the Al 7075 aluminum alloy were used for the verification of the proposed unified fatigue crack growth model. The method can be also used to predict fatigue crack growth under constant amplitude and spectrum loading in various environmental conditions such as vacuum, air, and corrosive environment providing that appropriate limited constant amplitude fatigue crack growth data obtained in the same environment are available. The proposed methodology is equally suitable for fatigue analysis of smooth, notched, and cracked components.

I. INTRODUCTION

ONE of the difficulties arising while modeling the fatigue crack growth (FCG) process is sufficiently accurate estimation of elastic–plastic stresses and strains ahead of the crack tip, resulting from the stress concentration and cyclic plastic deformation of the material volume in the crack tip region. Due to the presence of irreversible cyclic plastic deformations at the crack tip, significant compressive residual stresses are induced around the crack tip by cyclic and entirely tensile applied remote stresses or loads. Therefore, it is necessary to determine and account for the effect of the actual crack tip stresses and strains induced by previous loading cycles on fatigue crack growth rate caused by the current loading cycle. Most of the existing fatigue crack growth models emphasize the effect of the applied remote or nominal stress range without direct relation to the crack tip stress–strain affairs.

However, there are several difficulties with appropriate stress–strain modeling of the crack tip region and subsequent analysis of crack tip stresses and strains based on the continuum mechanics. The classical elastic[1] and elastic–plastic fracture mechanics solutions[2,3] concerning stresses and strains at the crack tip were derived for an ideal sharp crack having a tip radius $\rho^* = 0$. Such a model of the crack tip results in a singular solution with unrealistically high strains and stresses in the vicinity of the crack tip. In spite of the importance of these fundamental fracture mechanics solutions, they unfortunately cannot be directly used for the determination of the actual stresses and strains in the vicinity of a crack tip.

In order to better understand the stress–strain material behavior near the crack tip region, several experimental studies have been recently carried out by Tai[4] (digital image correlation method), Croft[5] (X-ray diffraction method), and Livne.[6] The measured strain

---

S. MIKHEEVSKIY, Research Associate, and G. GLINKA, Professor, are with the Department of Mechanical Engineering, University of Waterloo, Waterloo, ON, N2L 3G1, Canada. Contact e-mail: smikheev@engmail.uwaterloo.ca E. LEE, Researcher, is with the Naval Air Warfare Center Aircraft Division, Patuxent River, MD 20670.

distributions near fatigue cracks are characterized by high gradients, but as expected the strains near the crack tip were finite. It has also been indicated[4] that measured strain distributions could be well described by continuum mechanics solutions if the crack tip is assumed blunt and ended with a small radius ρ^*. Moreover, experimental observations carried out by Withers[7] and Jones[8] suggest that just behind the tip, the crack stays open even if the remaining area away from the crack tip is in contact. A similar small but open region just behind the fatigue crack tip was found while analyzing the crack opening displacement fields obtained from Finite Element analyses reported in References 9 and 10. This effect can be explained by the fact that plastically deformed material at the vicinity of a crack tip acts during unloading as an obstacle or a small rigid ball and prevents the region behind the crack tip from being closed.

Therefore, the crack tip in the fatigue crack growth analysis outlined below has been modeled as a sharp notch with a small but finite radius ρ^*. The advantage of using the blunt crack model lies in the fact that notch theories and continuum mechanics principles and solutions can be applied and the calculated crack tip stresses and strains become more realistic.

A. Basic Assumptions

Based on the experimental and numerical data discussed above, a fatigue crack growth model has been developed. It has been assumed (Figure 1) that fatigue crack can be modeled as a notch or blunt crack with the tip radius ρ^*. While unloading from the maximum stress to the stress level B (Figure 1), the plastically deformed material prevents the crack tip from being closed because the multi-axial stress state ahead of the crack tip significantly prevents reversed plastic deformation. Therefore, the crack surfaces may come into contact (closure) away from the crack tip, but the region just behind the crack tip remains open. For this reason, the contact stresses resulting from the often postulated crack closure phenomenon cannot be very effective because they are applied away from the crack tip. Experiments[8] and finite element analyses[10] also suggest that the contact stresses resulting from eventual crack closure are too small to be responsible for the stress ration (R-ratio) effect and fatigue crack growth retardation under spectrum loading. In addition, the experimental and numerical analyses[5,8,10] indicate that changes of the R-ratio or the overload effect are mainly manifested in the change of crack tip stresses and strains corresponding to the maximum stress intensity factor. This is contrary to the crack closure concept[11] suggesting that the R-ratio and the stress history effects are mainly due to the change of the effective minimum stress intensity factor and, subsequently, crack tip stresses and strains corresponding to the minimum stress intensity factor. Unfortunately, there were no data available until recently showing the link between the crack closure and the strain and stress evolution ahead of the crack tip. For this reason, the proposed model is concerned mainly with the analysis of cyclic elastic–plastic stresses and

strains ahead of the crack tip and the crack closure is not explicitly considered. When fully compressive remote stress or load is applied (below the zero level C in Figure 1), the crack, according to the model, is transformed into one or two holes of radius ρ^*. Such a transformation makes it possible to rationally account for the effect of the compressive part of a stress/load cycle. A detailed description of the model, named as the UniGrow model, has been presented in References 12–15. Therefore, only the main elements of the model are briefly described below.

The model is based on the idea that the fatigue process near cracks and notches is governed by highly concentrated strains and stresses in the small region adjacent to the crack/notch tip. Therefore, the fatigue crack growth can be subsequently considered as a process of successive crack increments resulting from the material damage in the crack tip region. It was subsequently assumed that the real material can be modeled as a set of elementary particles or material blocks (Figure 2) of finite dimension "ρ^*" and the crack has also the tip radius equal to "ρ^*." It is possible to assume a different material block size than "ρ^*," but the theoretic analysis and the final general form of the fatigue crack growth expression will not change. Therefore, the crack tip radius and the material block size are the same in the analysis presented below.

Because the crack tip has well-defined curvature, the usual notch stress–strain analysis techniques can be applied to determine stresses and strains in the crack tip region. The following assumptions and computational rules form the base for the UniGrow fatigue crack growth model.

- The material consists of elementary blocks (Figure 1) of a finite dimension "ρ^*."
- The fatigue crack is regarded as a deep notch with a finite tip radius "ρ^*."
- The stress–strain analysis is based on the cyclic Ramberg–Osgood[16] material stress–strain curve.

$$\varepsilon = \frac{\sigma}{E} + \left(\frac{\sigma}{K'}\right)^{\frac{1}{n'}} \qquad [1]$$

- The number of cycles necessary to fracture the material over the distance "ρ^*" ahead of the crack tip can be obtained using the Manson–Coffin[17,18] strain–life curve.

$$\frac{\Delta\varepsilon}{2} = \frac{\sigma_f'}{E}(2N_f)^b + \varepsilon_f'(2N_f)^c \qquad [2]$$

- The cumulative fatigue damage concept and the Smith–Watson–Topper[19] fatigue damage parameter.

$$DP = \frac{\Delta\varepsilon}{2}\sigma_{max} \qquad [3]$$
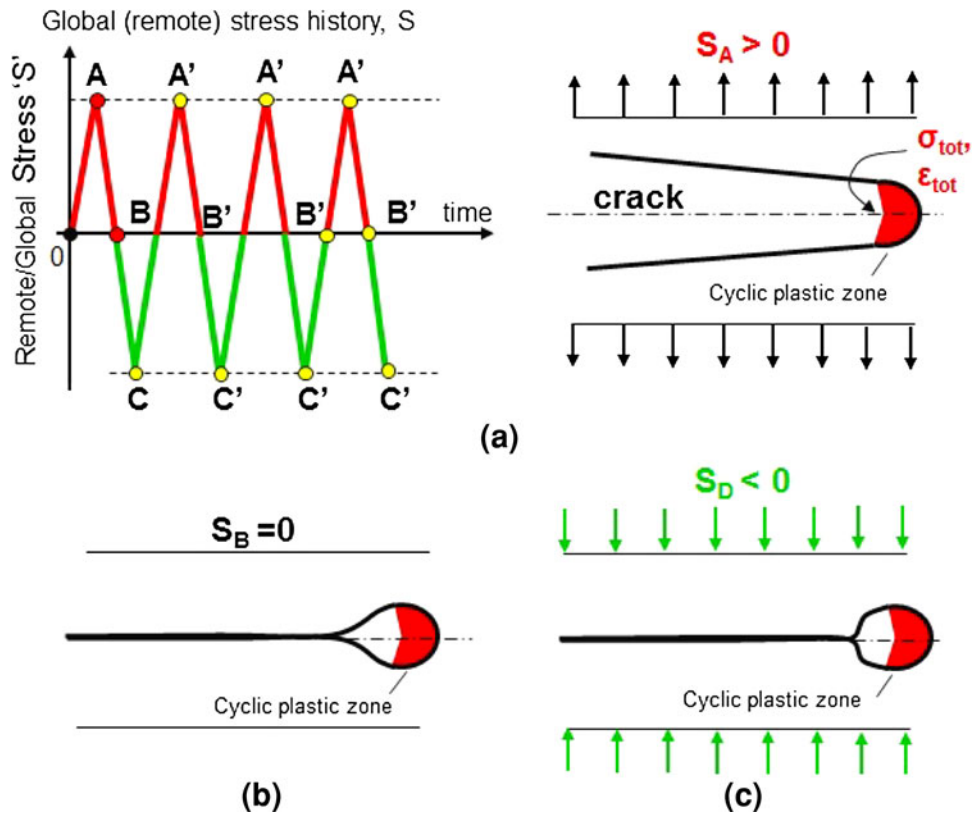
Fig. 1—Crack tip deformation under applied load.
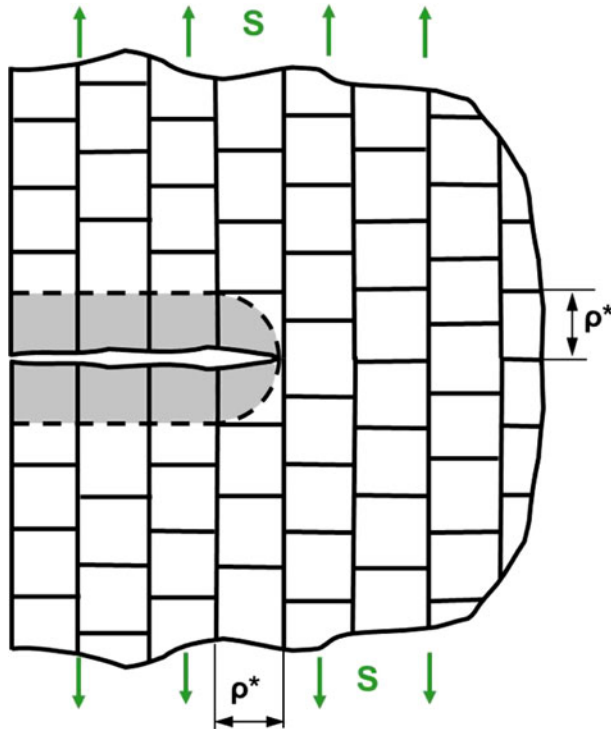
Fig. 2—Idealized discrete material model.

Based on the assumptions above, Noroozi and Glinka[12] have analytically derived the fatigue crack growth expression in the form of expression (4).

$$\frac{da}{dN} = C\left(\Delta K_{\text{tot}}^{1-p} K_{\text{max,tot}}^{1-p}\right)^{\gamma}$$
$$= C\left[\left(\Delta K_{\text{appl}} + K_{\text{r}}\right)^{1-p}\left(K_{\text{max,appl}} + K_{\text{r}}\right)^{p}\right]^{\gamma} \quad [4]$$

where

$$p = \frac{n'}{1 + n'}$$

Parameters "$K_{\text{max,appl}}$" and "$\Delta \Lambda_{\text{appl}}$" are the applied maximum stress intensity factor and the stress intensity range, respectively, and "K_{r}" is the residual stress intensity factor accounting for the effect of the crack tip residual stresses resulting from reversed plastic deformations. Parameters "p," "C," and "γ" are material constants. It has to be noticed that material constants "C" and "γ" depend on environmental conditions. The residual stress distribution "σ_{r}" ahead of the crack tip, dependent on the material elastic–plastic behavior and the cyclic stress/load history, was determined using the multi-axial Neuber rule discussed in References 20–22. The stress intensity factor K_{r}

induced by the residual stress "σ_r" was calculated using the universal weight functions[23,24] method.

The analytically derived Eq. [4] indicates that the fatigue crack growth rate depends on two basic load parameters "ΔK" and "K_{max}" as postulated earlier[25] by Sadananda and Vasudevan. A similar empirical fatigue crack growth expression was also proposed earlier by Walker[26] and Kujawski[27] based on observations of constant amplitude fatigue crack growth data obtained at various stress ratios "R." However, Walker's and Kujawski's expressions use only the applied stress intensity factors and, besides the fact that the mathematical expressions are similar, the use of the stress intensity factors corrected for the effect of residual stress makes the proposed model profoundly different as it can account for the stress history effect. Therefore, the determination of residual stresses around the moving crack tip, produced by subsequent stress/loading cycles, and their effects on the resultant (total) stress intensity factors, "ΔK_{tot}" and "$K_{max,tot}$," becomes one of the most important parts of the UniGrow model.

The elementary material block size, ρ^*, is one of the essential parameters of the UniGrow model. Several ways of estimating ρ^* can be found in[28] including the method based on material fatigue limit and threshold stress intensity factor range, the method based on strain–life experimental data for smooth specimen, and the method based on the constant amplitude fatigue crack growth data. The last method is used in the current paper since it provides not only the value of ρ^*, but also estimates material fatigue crack growth rates' parameters "C" and "γ." The ongoing research shows that ρ^* does depend on the material true strength and the statistically largest grain size. Additionally, it has to be noticed that the assumption of crack increment being equal to r^* is only used to analytically derive the form of total driving force, and the fatigue crack growth analysis is based on a cycle by cycle approach. Therefore, the r^* parameter is used only to define the local stresses and strains ahead of the crack (sharp notch) tip and the corresponding residual stress intensity factor.

B. Residual Stresses and Stress Intensity Factor

The residual stress distribution ahead of a growing fatigue crack due to one cycle of load was determined in two stages. First, the linear elastic stress distribution was determined using the Creager–Paris solution[29] for blunt cracks.

$$
\begin{aligned}
\sigma_{xx}^{el}(x) &= \frac{K}{\sqrt{2\pi x}}\left(-\frac{\rho^*}{2x}+1\right) \\
\sigma_{yy}^{el}(x) &= \frac{K}{\sqrt{2\pi x}}\left(\frac{\rho^*}{2x}+1\right) \\
\tau_{xy}^{el}(x) &= 0
\end{aligned}
\tag{5}
$$

Second, the elastic–plastic strains and stresses were calculated based on the pseudo-elastic stresses (5), the elastic–plastic material curve (1), and the multi-axial Neuber rule (6) described in References 21 and 22.

$$
\sigma_{ij}^{el}\varepsilon_{ij}^{el} = \sigma_{ij}^{a}\varepsilon_{ij}^{a}
\tag{6}
$$

The residual stresses "σ_r" were determined over a series of elementary material blocks, as shown in Figure 3, resulting in a stress distribution given by a series of stress values $\sigma_r(x_i)$. The resultant residual stress distribution which consists of all the residual stress distributions produced through the loading spectrum (Figure 4) and the universal weight function $m(x)$ enabled the calculation[23,24] of the residual stress intensity factor K_r.

$$
K_{res} = \int_0^a \sigma_r(x)\, m(x,a)\, dx
\tag{7}
$$

where

$$
m(x,a) = \frac{2}{\sqrt{2\pi(a-x)}}\left[1 + M_1\left(1-\frac{x}{a}\right)^{\frac{1}{2}} + M_2\left(1-\frac{x}{a}\right)^{1} + M_3\left(1-\frac{x}{a}\right)^{\frac{3}{2}}\right]
$$

Geometrical parameters M_1, M_2, M_3, of various weight functions can be found in References 23 and 24.

The minimum and maximum stress intensity factors induced by the applied fluctuating nominal stress $S_{appl,max}$ and $S_{appl,min}$ can be calculated using ready-made handbook solutions

$$
K_{max,appl} = S_{max,appl}\sqrt{\pi a}\,Y; \quad K_{min,appl} = S_{min,appl}\sqrt{\pi a}\,Y
\tag{8}
$$

or the same weight function and appropriate stress distribution[23,24] induced by the externally applied cyclic load.

One of the essential questions was how the residual stress intensity factor K_r should be combined with the applied stress intensity factors $K_{max,appl}$ and $K_{min,appl}$ to appropriately model the effect of the residual stress and, subsequently, the stress history effect. Therefore, a series of experiments were carried out[5] to measure strains around the growing fatigue crack tip before and after single overload. In addition, finite element analyses were also carried out[10] for the same material, specimen geometry, and loading history. The experimental and numerical data have revealed that the residual stresses influenced the crack tip strains and stresses much more at the maximum load rather than the minimum, resulting in simultaneous decrease of the resultant range and maximum stress intensity factors. Therefore, the residual stress intensity factor K_r is combined with both the range ΔK_{appl} and the maximum applied stress intensity factor $K_{max,appl}$ according to Eq. [4]. This approach differs from the popular opinion that only the minimum stress intensity $K_{min,appl}$ should be raised because of the crack closure phenomenon.
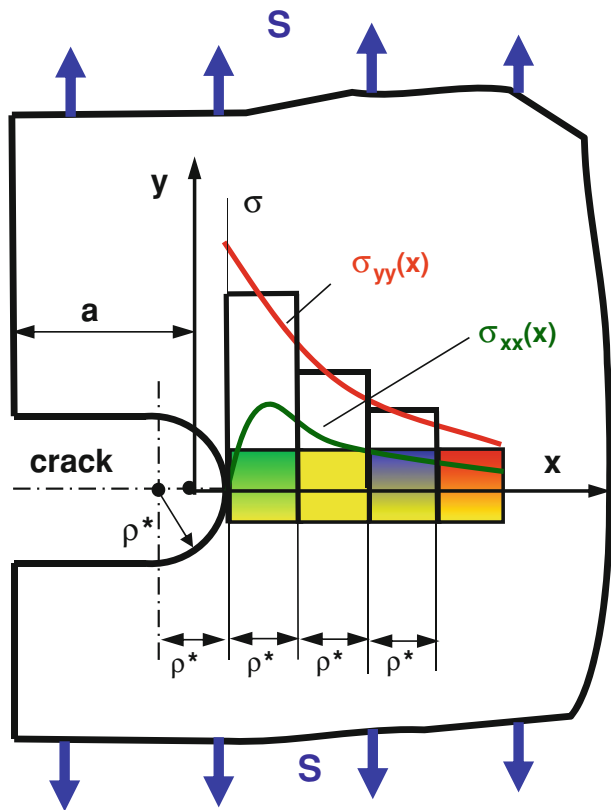
Fig. 3—Discrete stress distribution ahead of the crack tip.
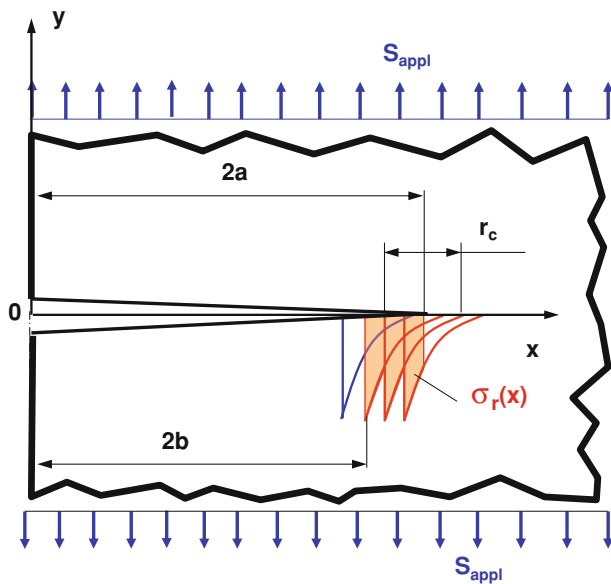
Fig. 4—Resultant residual stress distribution.

C. Memory Rules

The residual stresses are calculated after each stress reversal. However, the effect of residual stress distributions created by previous stress cycles depends on the current position of the crack tip relative to the crack tip position when past cycles created previous stress fields.

Therefore, it was necessary to estimate for how long stress distributions created by past cycles are influencing the residual stress intensity factor K_r for the crack tip at the current position. In other words, it is necessary to define when the effect of the previous cycle (or cycles) can be neglected because the crack tip has propagated out of its zone of influence.

Based on the analysis of various literature and in-house experimental fatigue crack growth data, a set of rules was formulated[14] with the purpose of accounting for the effect of magnitude, distribution, and the longevity of effectiveness of residual stresses created ahead of growing fatigue cracks. Four rules have been subsequently formulated for the determination of the residual stress intensity factor required for the estimation of the instantaneous fatigue crack growth rate and crack increments induced by individual stress/load cycles. According to the proposed methodology, all stress distributions induced by previous cycles, relative to the current crack tip position, have to be combined into one resultant residual stress field for the residual stress intensity factor Kr to be determined.

- First, only the compressive part of the residual crack tip stress field corresponding to the minimum applied stress/load affects the fatigue crack growth rate.
- Second, if the compressive part of the stress distribution corresponding to K_{min} of the current loading cycle is completely inside the previous resultant minimum stress field, the material does not "feel" it and the current minimum stress distribution should be neglected.
- Third, if the compressive part of the minimum stress distribution of the current loading cycle is fully or partly outside the previous resultant minimum stress field, they should be combined.
- The fourth rule states that each minimum stress distribution should be included into the resultant one only when the crack tip is inside its compressive stress zone. In other words, when the crack tip has propagated across the entire compressive stress zone of the current minimum stress field, it should be neglected or deleted from the resultant residual stress field.

All four rules are schematically explained in Figure 5. Part "a" shows a variable amplitude loading history. The corresponding residual stress profile is presented in part "b." Loading cycles with a higher range produce more damage; however, they also create a large compressive stress field ahead of the crack tip. It causes the decrease of the residual stress intensity factor "K_r" and subsequent decrease of the FCG rate as shown in part "c." The highlighted region in part "b" shows residual stresses to be used for the residual stress intensity factor calculation K_r while the crack tip is at point A. Compressive stress fields induced by small cycles occurring between two subsequent overloads are neglected (the second rule) and the stress field due to the first cycle is excluded (the fourth rule).
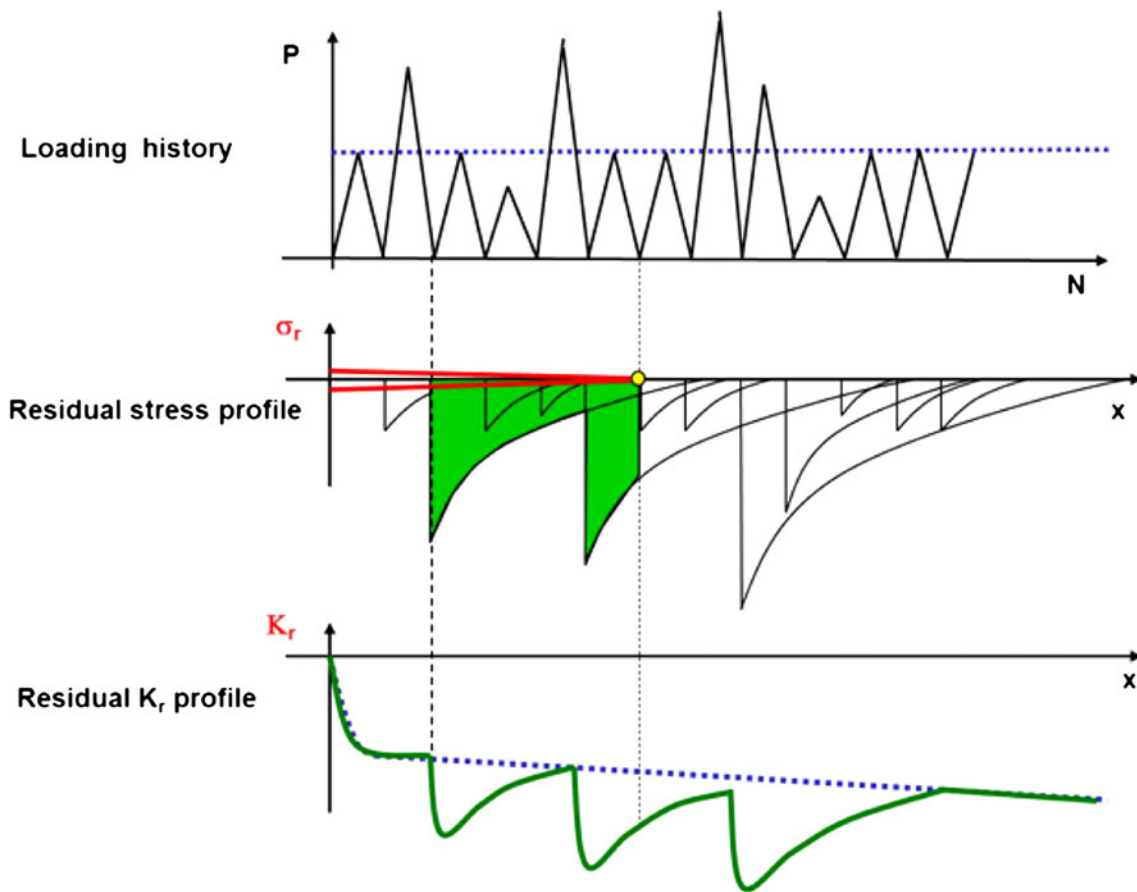
Fig. 5—Compressive residual stress fields induced by subsequent load cycles of a spectrum loading; (*a*) loading history, (*b*) minimum residual stress fields, (*c*) residual stress intensity factor as a function of the crack tip position.

II. ENVIRONMENTAL EFFECTS ON FCG

According to the UniGrow fatigue crack growth model, the FCG analysis under variable amplitude loading in particular environment should be based on constant amplitude FCG data obtained in the same environment. Other words, it is assumed that material resistivity to FCG is changing (increasing or decreasing) in a corrosive environment, but the mechanical component of FCG driving force remains the same. This idea is supported by the set of experiments performed by Lee.[30] It has been shown that material strain–life (ε–N) response changes dramatically depending on different environmental conditions; however, the material cyclic stress–strain curve (σ–ε) is almost insensitive to environmental changes (Figure 6). All experiments required for determination of stress–strain, strain–life, and fatigue crack growth material constants have been performed under a relatively slow frequency of 10 Hz. The variable loading history used for fatigue crack growth analysis was applied under a similar frequency of 5 Hz.

Similarly, material constants "*C*" and "*γ*" in Eq. [1], characterizing the resistivity to FCG, depend on the Manson–Coffin strain–life curve parameters. Therefore, the recommended method of estimation of the FCG constants (Eq. [4]) and the elementary material block

size "*ρ**" based on the Manson–Coffin and the Ramberg–Osgood material curves includes indirectly the effect of the environment in the UniGrow model and enables the prediction of fatigue crack growth in corrosive environments, providing that the basic reference material curves (ε–N) and (σ–ε) obtained in a given environment are available.

The fatigue crack growth behavior of Al 7075-T651 alloy was investigated by Lee[29] under constant amplitude loading (frequency 10 Hz) in three different environments (vacuum, air 70 pct RH, and 1 pct NaCl solution). A similar set of experiments has been also performed by Pao.[31] The FCG rate as a function of the applied stress intensity range is shown in Figure 7. As expected, the slowest crack growth rate was observed in vacuum and the highest in 1 pct NaCl solution.

The constant amplitude datasets shown in Figure 7 enable the estimation of the crack tip radius "*ρ**" for all three environments. Since the mean stress effect in Eq. [4] has been accounted for using the SWT damage parameter, each set of experimental FCG rate data points plotted as a function of the two-parameter driving force, $\Delta\kappa = K^{p}_{\mathrm{max,tot}}\Delta K^{(1-p)}_{\mathrm{tot}}$, should collapse onto one "master" curve. On the other hand, the two-parameter driving forces "$\Delta\kappa_{\mathrm{tot}}$" can be determined as a function of the crack tip radius "$\rho*$," which depends on the environment.
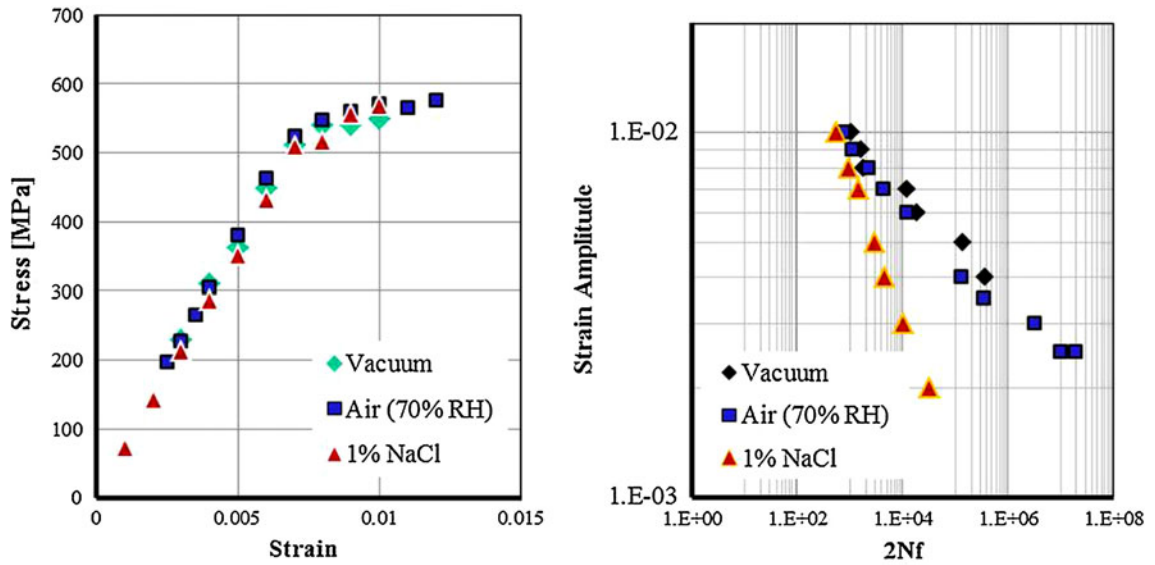
Fig. 6—Strain-Stress and Strain-Life behavior of Al 7075-T6 in different environments.
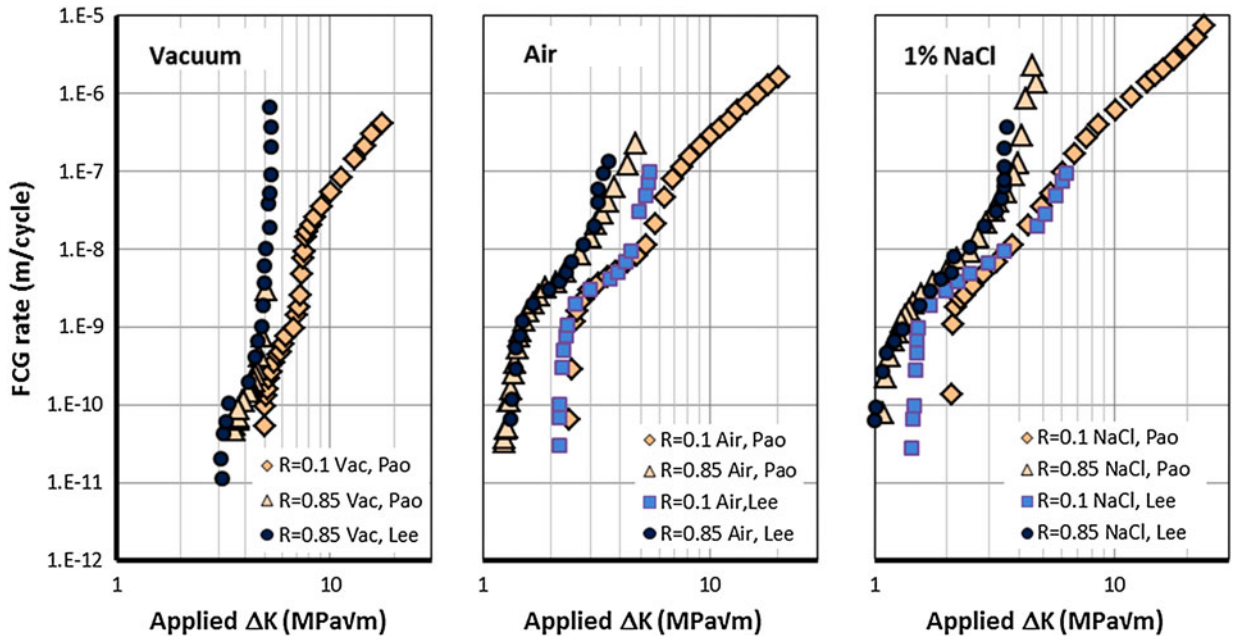
Fig. 7—FCG rates as a function of applied SI range for vacuum, air, and NaCl.

$$\Delta\kappa = K_{max,tot}^{p}\Delta K_{tot}^{(1-p)}$$
$$= \left(K_{max,appl}^{p} + K_r\right)^{p}\left(\Delta K_{appl} + K_r\right)^{1-p}$$
$$= \left(K_{max,appl}^{p} + \int_0^a \sigma_r(x|\rho*) \cdot m(a,x)dx\right)^{p}$$
$$\times \left(\Delta K_{appl} + \int_0^a \sigma_r(x|\rho*) \cdot m(a,x)dx\right)^{1-p}$$
$$= \Delta\kappa(\rho*)$$

where $\sigma_r(x|\rho*)$ is the residual stress field due to cyclic plasticity, "a" is the current crack length, and $m(a,x)$ is the weight function appropriate for the given geometry.

Since the crack tip radius "$\rho*$" is the only unknown parameter in the equation above, it has to be selected in such a way that all experimental constant amplitude FCG data points, obtained at various stress ratios R, collapse onto one $da/dN - \Delta\kappa_{tot}$ "master" curve. The resultant $da/dN - \Delta\kappa_{tot}$ "master" curves for all three environments are shown in Figure 8. The collapsed "master" FCG rate curves presented in terms of the
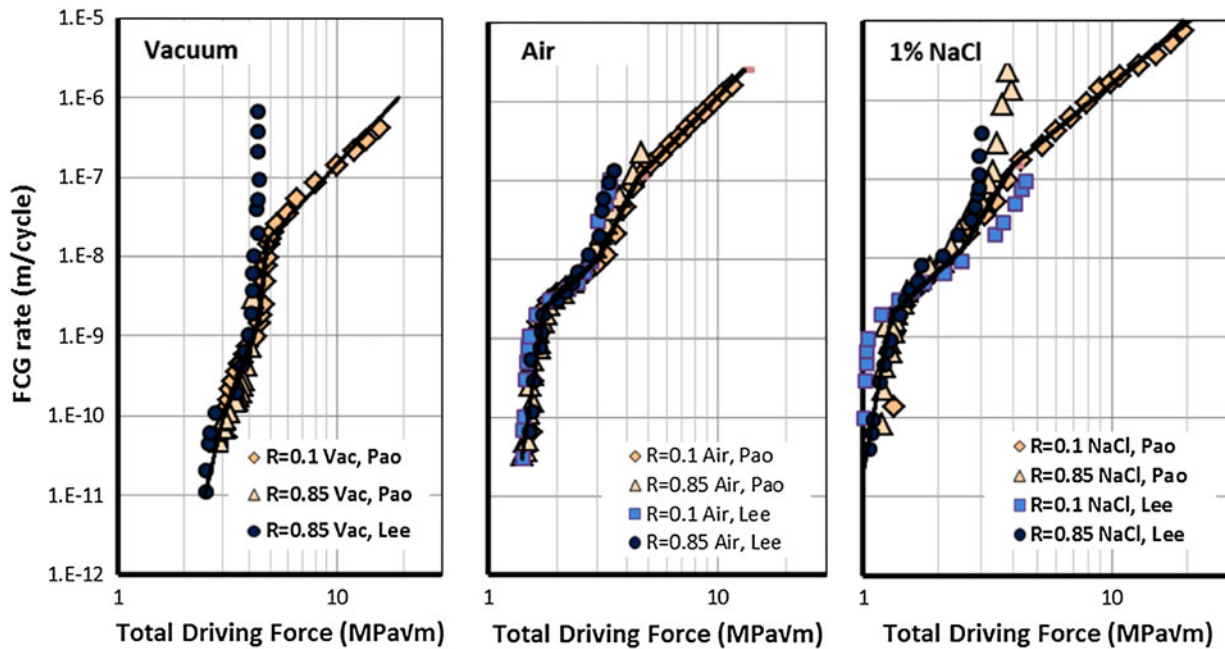
Fig. 8—FCG rates as a function of total driving force for vacuum, air, and NaCl.

Table I. Elementary Material Block Sizes for Different Environments (Al 7075-T6)

Environment	Elementary Material Block Size
Vacuum	2.0e−6 m
Laboratory air	3.8e−6 m
1 pct NaCl solution	4.5e−6 m

total driving force, "$\Delta\kappa_{tot}$" were divided into four segments and each segment was subsequently approximated by a straight line fitted into the experimental data points using the linear regression method. The estimated values of elementary material block size "ρ^*" for different environments are shown in the following Table I.

As one may notice, the lowest value corresponds to vacuum and the highest one corresponds to 1 pct NaCl solution. It makes sense since, according to the proposed model, the elementary material block size, ρ^*, is proportional to the instantaneous fatigue crack growth rate, da/dN,[12] which follows the same trend.

The experimental data for high R-ratio in vacuum show huge increase of fatigue crack growth rates, da/dN, when applied stress intensity range approaches certain value (5 MPa√m). It might happen because the maximum applied stress intensity factor approached fracture toughness. In this case, the crack growth is caused not only by applied cyclic load but by static fracture as well. Similar explanation may be used to justify the deviation of experimental fatigue crack growth data for R = 0.85 from collapsed material curve in NaCl (Figure 8).

A. Variable Loading

The central through crack specimens were used to investigate the effect of the environment on FCG in Al 7075 to 7651 alloy under variable amplitude loading. The specimens were 102 mm wide, 235 mm long, and 2 mm thick with a 3-mm radius central notch from which the crack starters were cut. More detailed description of the specimens and the testing procedure can be found in the original work by Lee.[29]

The variable amplitude fatigue loading tests and UniGrow fatigue life predictions were performed under two different types of loading spectra: tension dominated and tension–compression. The following table gives the maximum/minimum stresses and the number of reversal for each spectrum.

	Maximum Stress (MPa)	Minimum Stress (MPa)	Number of Cycles (MPa)
Tension Dominated	200.9	−73.7	2,249,614
Tension–Compression	162.3	−163.7	1,975,035

The test conditions for variable amplitude fatigue crack growth tests were vacuum at 4e−8 T, laboratory air with relative humidity 50 pct, and 1 pct NaCl solution. The average loading frequency was around 5 Hz.

III. EXPERIMENTAL RESULTS AND UNIGROW PREDICTIONS

The predicted and experimental crack length *vs* number of cycles' (*a–N*) datasets for the tension–compression
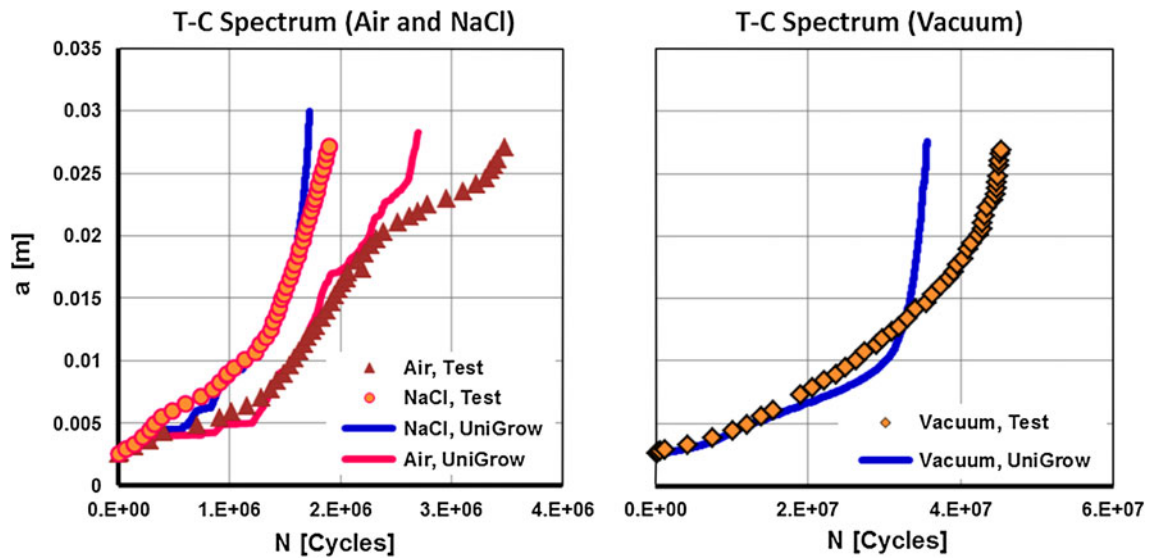
Fig. 9—FCG predictions and experimental data for air, 1 pct NaCl, and vacuum under tension–compression loading spectrum.
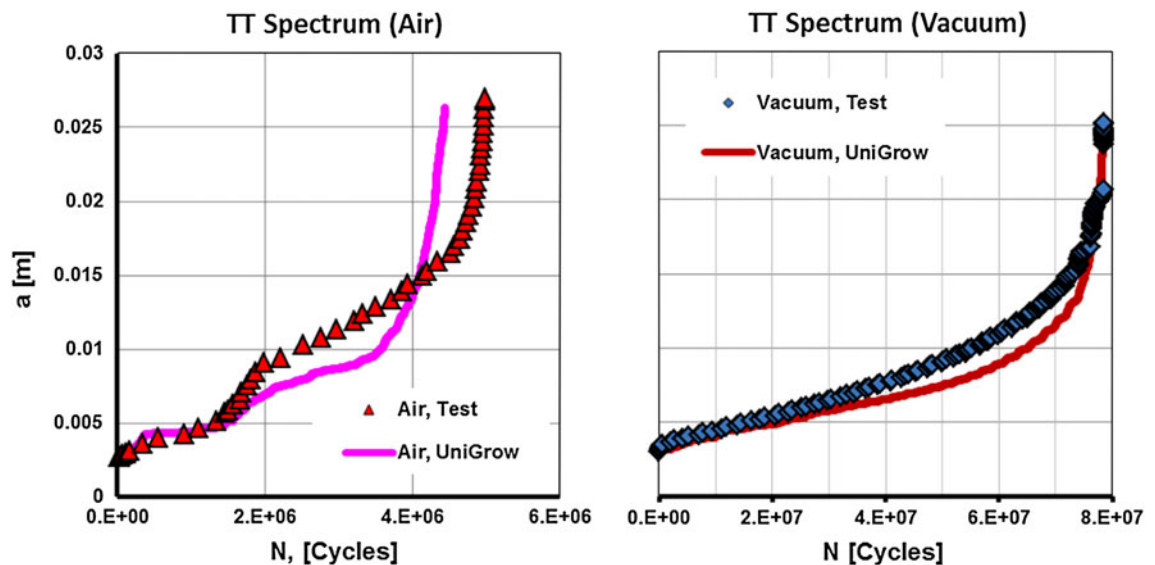
Fig. 10—FCG predictions and experimental data for air, 1 pct NaCl, and vacuum under tension-dominated loading spectrum.

loading spectrum are shown in Figure 9. The experimental measurements show that the fatigue life in vacuum is much longer (~43 million cycles) than in air (3.5 million cycles), which coincides well with constant amplitude FCG data. Similarly, the fatigue life measured in 1 pct NaCl solution is about twice shorter than in air (1.7 million).

An interesting observation can be made based on the shape of the FCG curve in each particular environment. Both air and 1 pct NaCl solution curves have a step-wise shape with distinct multiple retardation plateau and intervals of high FCG rates. The retardation effects are due to the large plastic deformations at the vicinity of a crack tip produced by high overloading cycles. However, these effects are less visible in the 1 pct NaCl solution. It can be explained by the fact that the total FCG driving force depends not only on the mechanical

driving force and the plastic deformations around the crack, but also on the corrosion mechanisms. On the contrary, in the vacuum, the experimental FCG curve has a traditional smooth shape with no visible retardation or acceleration effects.

The UniGrow FCG model gives good estimation of fatigue lives in all three environments (Figure 9). The theoretic a–N curves not only match the final fatigue lives, but also follow the same shapes as it was measured in the experiments. The difference in fatigue life between experimental data and theoretic predictions may come from the scatter of constant amplitude fatigue crack growth data used to estimate the elementary material block size, ρ^*, and material/environmental constants, C and γ.

The theoretical predictions and experimental measurements for tension-dominated loading spectrum in

air and vacuum are show in Figure 10. Similar to the results discussed above, the fatigue life in vacuum is approximately 10 times longer than in air and the shapes of FCG curves are different.

It should be noted that the fatigue life under the tension-dominated spectrum is approximately 30 pct longer than under the tension–compression spectrum in air and 100 pct longer in vacuum. This result could be anticipated because the compressive part of the cycle may eliminate the retardation effect induced by high overload cycles. In other words, in the case of the tensile loading spectrum (no underloads), the residual stress retardation effect was much greater than in the case of the tension–compression spectrum. A similar effect was observed by Kujawski[27] in air. The difference in fatigue lives (experimental and theoretic) under tension-dominated and tension–compression loading spectra was more significant in vacuum than in air. Figure 9 shows the ability of the UniGrow model to predict life under loading spectrum containing large compressive underloads.

The similar estimation of fatigue life under tension-dominated loading spectrum using UniGrow model has been shown by Lee.[29] However, he fitted two-pieces fatigue crack growth rate curve into collapsed data (Figure 8), which resulted in ~$2e+7$ difference in the final fatigue life. Additionally, the elementary material block size parameter, r^*, was defined in Reference 29 using a simplified equation proposed by Noroozi.[12] The current approach to estimate R^* is described above in the "Environmental effects on FCG" section.

In spite of the fact that the UniGrow fatigue crack growth model gives a very good estimation of fatigue life, one can notice that predicted fatigue crack growth rates are sometimes lower and sometimes higher than experimental ones (Figure 9 and Figure 10). It can be explained by the fact that retardation effects of high overloads are not always estimated correctly because of inaccuracy of the applied model for elastic–plastic stress–strain behavior (Neuber rule). It has been shown that the multi-axial Neuber rule gives a good estimation of elastic plastic stresses and strains[21] in the vicinity of a crack tip; however, it is still just an approximation.

IV. CONCLUSIONS

The analysis presented above shows that various effects influencing fatigue crack growth resulting from the application of cyclic variable amplitude loading in different environmental conditions can be modeled by considering the influence of residual stresses caused by reversed cyclic plastic deformation in the crack tip region and using as a base the FCG constant amplitude data for the particular environment.

It has been shown that the retardational effect induced by high overloads is more visible in air, where the FCG is influenced mostly by mechanical driving force and residual stresses, and less visible in 1 pct NaCl, where the chemical effects are present.

It has also been shown that the use of the "memory rules" and the two-parameter UniGrow driving force enables realistic simulation of the fatigue lives of cracked bodies subjected to complex variable amplitude service loading spectra.

REFERENCES

1. G. R. Irwin: in *Handbuch der Physik*, S. Flügge, ed., Springer, Berlin, 1958.
2. J.R. Rice and G.F. Rosengren: *J. Mech. Phys. Solids*, 1968, vol. 16 (4), pp. 1–12.
3. J.W. Hutchinson: *J. Mech. Phys. Solids*, 1968, vol. 16 (4), p. 13.
4. Y.H. Tai and J.R. Yates: *Int. Conf. on Characterization of Crack Tip Stress Fields*, Forni di Sopra (UD), Italy, March 7–9, 2011, pp. 230–35.
5. M. Croft, Z. Zhong, N. Jisrawi, I. Zakharchenko, R.L. Holtz, J. Skaritka, T. Fast, K. Sadananda, M. Lakshmipathy, and T. Tsakalakos: *Int. J. Fatigue*, 2005, vol. 27, pp. 1408–19.
6. A. Livne, E. Bouchbinder, I. Svetlizky, and J. Fineberg: *Science*, 2010, vol. 327 (5971), pp. 1359–63.
7. P.J. Withers, H. Dai, and P. Lopez-Crespo: *Int. Conf. on Characterization of Crack Tip Stress Fields*, Forni di Sopra (UD), Italy, March 7–9, 2011.
8. R. Jones, M. Krishnapillai, K. Cairns, and N. Matthews: *Fatig. Fract. Eng. Mater. Struct.*, 2010, vol. 33, pp. 871–84.
9. J. Zhang, X.D. He, B. Suo, and S.Y. Du: *Eng. Fract. Mech.*, 2008, vol. 75, pp. 5217–28.
10. G. Glinka, A. Buczynski: *Int. Conf. on Characterization of Crack Tip Stress Fields*, Forni di Sopra (UD), Italy, March 7–9, 2011.
11. J.C. Newman: *Methods and Models for Predicting Fatigue Crack Growth under Random Loading*, ASTM STP 748, Philadelphia, 1981, pp. 53–84.
12. A.H. Noroozi, G. Glinka, and S. Lambert: *Int. J. Fatigue*, 2005, vol. 27, pp. 1277–96.
13. A.H. Noroozi, G. Glinka, and S. Lambert: *Int. J. Fatigue*, 2007, vol. 29, pp. 1616–33.
14. S. Mikheevskiy and G. Glinka: *Int. J. Fatigue*, 2009, vol. 31, pp. 1828–36.
15. S. Mikheevskiy, G. Glinka, and D. Algera: *Int. J. Fatigue*, 2012, vol. 42, pp. 88–94.
16. C.C. Osgood: *Fatigue Design*, Pergamon Press, New York, 1982.
17. L. Coffin: *Trans Am Soc Mech Eng*, 1954, vol. 76, pp. 931–50.
18. S.S. Manson and G.R. Halford: *Fatigue and Durability of Structural Materials*, ASM International, Materials Park, OH, 2006.
19. K.N. Smith, P. Watson, and T.H. Topper: *J. Mater.*, 1970, vol. 5 (4), pp. 767–78.
20. H. Neuber: *J. Appl. Mech. ASME*, 1961, vol. 28, pp. 544–550.
21. A. Moftakhar, A. Buczynski, and G. Glinka: *Int. J. Fract.*, 1995, vol. 70, pp. 357–73.
22. M.N.K. Singh, G. Glinka, and R.N. Dubey: *Int. J. Fract.*, 1996, vol. 76, pp. 39–60.
23. G. Glinka and G. Shen: *Eng. Fract. Mech.*, 1991, vol. 40 (6), pp. 1135–46.
24. Z. Wu, G. Glinka, H. Jakubczak, and L. Nilsson: *J. ASTM Int.*, 2004, vol. 1 (9), pp. 1–14.
25. N. Louat, K. Sadananda, M. Duesbery, and A.K. Vasudevan: *Scripta Metall.*, 1993, vol. 28, pp. 65–70.
26. E.K. Walker: *Effect of Environment and Complex Load History on Fatigue Life*, ASTM STP 462, Philadelphia, 1970, pp. 1–14.
27. S. Dinda and D. Kujawski: *Eng. Fract. Mech.*, 2004, vol. 71 (12), pp. 1779–90.
28. Mikheevskiy, PhD Thesis, University of Waterloo, 2009.
29. M. Creager and P.C. Paris: *Int. J. Fract.*, 1967, vol. 3, pp. 247–51.
30. E.U. Lee, G. Glinka, A.K. Vasudevan, N Iyyer, and N.D. Phan: *Int. J. Fatigue*, 2009, vol. 31, pp. 1858–64.
31. P.S. Pao: Naval Research Laboratory, Washington, DC, private communication, 2011.